

# Topological Insulators in Three Dimensions

Liang Fu, C.L. Kane and E.J. Mele

*Dept. of Physics and Astronomy, University of Pennsylvania, Philadelphia, PA 19104*

We study three dimensional generalizations of the quantum spin Hall (QSH) effect. Unlike two dimensions, where the QSH effect is distinguished by a single  $Z_2$  topological invariant, in three dimensions there are 4 invariants distinguishing 16 “topological insulator” phases. There are two general classes: weak (WTI) and strong (STI) topological insulators. The WTI states are equivalent to layered 2D QSH states, but are fragile because disorder continuously connects them to band insulators. The STI states are robust and have surface states that realize the 2+1 dimensional parity anomaly without fermion doubling, giving rise to a novel “topological metal” surface phase. We introduce a tight binding model which realizes both the WTI and STI phases, and we discuss the relevance of this model to real three dimensional materials, including bismuth.

PACS numbers: 73.43.-f, 72.25.Hg, 73.20.-r, 85.75.-d

In recent years, the advent of spintronics has motivated the study of the effects of spin orbit interactions (SOI) on the electronic structure of solids. SOI leads to the spin Hall effect[1, 2], which has been observed in GaAs[3, 4]. We proposed[5] that in graphene the SOI leads to the quantum spin Hall (QSH) effect. In the QSH phase there is a bulk excitation gap along with gapless spin-filtered edge states. The QSH phase is distinguished from a band insulator by a  $Z_2$  topological invariant[6], which is a generalization applicable to time reversal invariant systems of the TKKN invariant of the integer quantum Hall effect[7]. Because of the weak SOI in carbon, the SOI induced energy gap in graphene is likely to be quite small[8]. However, Murakami has recently suggested that bismuth bilayers may provide an alternative venue for the QSH effect[9]. This breakthrough provides a new direction for the experimental observation of this phase.

In this paper we consider the generalization of the QSH effect to three dimensions (3D). Our work builds on recent progress by Moore and Balents[10], who showed that time reversal invariant energy bands in 3D are characterized by four  $Z_2$  invariants, leading to 16 classes of “topological insulators”. A similar result has also been obtained by Roy[11]. Here, we will explain the physical meaning of these invariants and characterize the phases they distinguish. One of the four invariants is of special significance and distinguishes what we will refer to as “weak” and “strong” topological insulators. With disorder, the weak topological insulator (WTI) is equivalent to a band insulator, while the strong topological insulator (STI) remains robust. We show WTIs and STIs have surface states with an even and odd number of Dirac points respectively. The latter case leads to a new “topological metal” surface phase, which we characterize. We introduce a tight binding model on a distorted diamond lattice, which realizes both the WTI and STI phases, allowing the surface states to be studied explicitly.

In Ref. 12 we established the connection between the  $Z_2$  invariant for the bulk QSH phase and the spin filtered edge states. We begin by reviewing that argument in a

way which makes the generalization to 3D transparent. The 2D invariant can be understood using a Laughlin type construction[13] on a cylinder threaded by magnetic flux  $\Phi = 0$  or  $\pi$  (in units of  $\hbar/e$ ). The invariant characterizes the change in the *time reversal polarization* (TRP), which signals the presence of a Kramers degeneracy at the ends, when  $\Phi$  is changed from 0 to  $\pi$ . If the cylinder consists of a single unit cell in the circumferential ( $x$ ) direction, then the magnetic flux threading the cylinder plays the role of the crystal momentum  $k_x$  in band theory. The spectrum of the discrete end states of the cylinder as a function of flux then reflects the edge state spectrum as a function of momentum. The change in the TRP as a function of flux determines the way the Kramers degenerate end states at the edge time reversal invariant momenta (TRIM)  $k_x = \Lambda_1 = 0$  and  $k_x = \Lambda_2 = \pi$  are connected to each other. In the QSH phase the Kramers pairs “switch partners” (Fig. 1a), reflecting the change in the TRP, while in the conventional insulator (Fig. 1b) they do not. It follows that in the QSH phase edge states traverse the bulk energy gap, and cross the Fermi energy an *odd* number of times between  $\Lambda_a$  and  $\Lambda_b$ . In the insulating phase, the edge states cross the Fermi energy an even number of times if at all. They are not topologically protected, since changes in the Hamiltonian at the edge can push the entire edge band out of the bulk gap.

The change in the TRP between  $\Lambda_1$  and  $\Lambda_2$  is related to the bulk band structure, defined for a 2D system with periodic boundary conditions in both directions. The 2D Brillouin zone has four TRIM,  $\Gamma_i$ , which are related to  $-\Gamma_i$  by a reciprocal lattice vector. For an edge perpendicular to  $\mathbf{G}$  the 1D edge TRIM  $\Lambda_{a=1,2}$  are projections of pairs  $\Gamma_{i=a1}$ ,  $\Gamma_{i=a2}$ , which satisfy  $\Gamma_{a1} - \Gamma_{a2} = \mathbf{G}/2$ , onto the line perpendicular to  $\mathbf{G}$ .

The TRP associated with  $\Lambda_a$  can be expressed as  $\pi_a = \delta_{i=a1}\delta_{i=a2}$ , where[12]

$$\delta_i = \sqrt{\text{Det}[w(\Gamma_i)]}/\text{Pf}[w(\Gamma_i)] = \pm 1. \quad (1)$$

Here the unitary matrix  $w_{ij}(\mathbf{k}) = \langle u_i(-\mathbf{k})|\Theta|u_j(\mathbf{k}) \rangle$ . At  $\mathbf{k} = \Gamma_i$ ,  $w_{ij} = -w_{ji}$ , so the Pfaffian  $\text{Pf}[w]$  is defined.  $\pi_a$  is

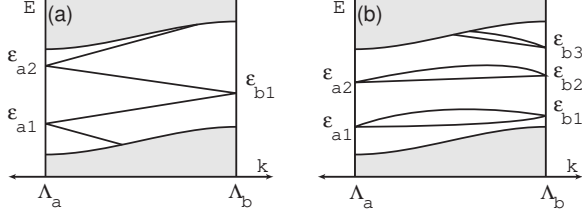


FIG. 1: Schematic surface (or edge) state spectra as a function of momentum along a line connecting  $\Lambda_a$  to  $\Lambda_b$  for (a)  $\pi_a \pi_b = -1$  and (b)  $\pi_a \pi_b = +1$ . The shaded region shows the bulk states. In (a) the TRP changes between  $\Lambda_a$  and  $\Lambda_b$ , while in (b) it does not.

free of the ambiguity of the square root in (1), provided the square root is chosen continuously as a function of  $\mathbf{k}$ . However,  $\pi_a$  is not gauge invariant. A  $\mathbf{k}$  dependent gauge transformation can change the sign of any pair of  $\delta_i$ 's. This reflects the physical fact that the end Kramers degeneracy depends on how the crystal is terminated. It is similar to the ambiguity of the charge polarization[12]. The product,  $\pi_1 \pi_2 = \delta_1 \delta_2 \delta_3 \delta_4$ , is gauge invariant, and characterizes the *change* in TRP due to changing the flux from  $\Lambda_1 = 0$  to  $\Lambda_2 = \pi$ . This defines the single  $Z_2$  invariant in 2D, and using the above argument, determines the connectivity of the edge state spectrum.

In 3D there are 8 distinct TRIM, which are expressed in terms of primitive reciprocal lattice vectors as  $\Gamma_{i=(n_1 n_2 n_3)} = (n_1 \mathbf{b}_1 + n_2 \mathbf{b}_2 + n_3 \mathbf{b}_3)/2$ , with  $n_j = 0, 1$ . They can be visualized as the vertices of a cube as in Fig. 2. A gauge transformation can change the signs of  $\delta_i$  associated with any four  $\Gamma_i$  that lie in the same plane. Modulo these gauge transformations, there are 16 invariant configurations of  $\delta_i$ . These can be distinguished by 4  $Z_2$  indices  $\nu_0; (\nu_1 \nu_2 \nu_3)$ , which we define as

$$(-1)^{\nu_0} = \prod_{n_j=0,1} \delta_{n_1 n_2 n_3} \quad (2)$$

$$(-1)^{\nu_{i=1,2,3}} = \prod_{n_j \neq i=0,1; n_i=1} \delta_{n_1 n_2 n_3}. \quad (3)$$

$\nu_0$  is independent of the choice of  $\mathbf{b}_k$ .  $(\nu_1 \nu_2 \nu_3)$  are not, but they can be identified with  $\mathbf{G}_\nu \equiv \sum_i \nu_i \mathbf{b}_i$ , which belongs to the 8 element *mod 2 reciprocal lattice*, in which vectors that differ by  $2\mathbf{G}$  are identified.  $(\nu_1 \nu_2 \nu_3)$  can be interpreted as Miller indices for  $\mathbf{G}_\nu$ .

$\nu_{0-4}$  are equivalent to the four invariants introduced by Moore and Balents using general homotopy arguments. The power of the present approach is that it allows us to characterize the surface states on an arbitrary crystal face. Generalizing the Laughlin argument to 3D, consider a system with open ends in one direction and periodic boundary conditions in the other two directions. This can be visualized as a torus with a finite thickness (a ‘‘Corbino donut’’), which has an inside and an outside surface. Viewed as a 1D system, we then seek to clas-

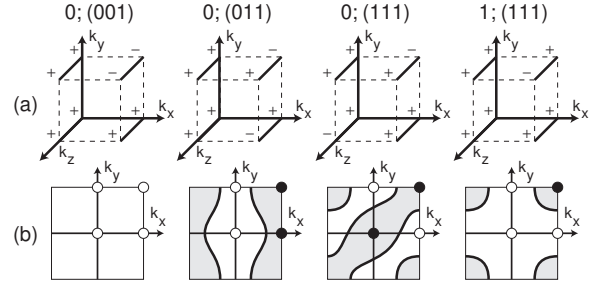


FIG. 2: Diagrams depicting four different phases indexed by  $\nu_0; (\nu_1 \nu_2 \nu_3)$ . (a) depicts  $\delta_i$  at the TRIM  $\Gamma_i$  at the vertices of the cube. (b) characterizes the 001 surface in each phase. The surface TRIM  $\Lambda_a$  are denoted by open (filled) circles for  $\pi_a = \delta_{a1} \delta_{a2} = +1 (-1)$ . They are projections of  $\Gamma_{a1}$  and  $\Gamma_{a2}$ , which are connected by solid lines in (a). The thick lines and shaded regions in (b) indicate possible surface Fermi arcs which enclose specific  $\Lambda_a$ .

sify the changes in the Kramers degeneracy associated with the surfaces as a function of two fluxes threading the torus (or equivalently as a function of the two components of the surface crystal momentum).

For a surface perpendicular to  $\mathbf{G}$ , the surface Brillouin zone has four TRIM  $\Lambda_a$  which are the projections of pairs  $\Gamma_{a1}, \Gamma_{a2}$ , that differ by  $\mathbf{G}/2$ , into the plane perpendicular to  $\mathbf{G}$ . Due to Kramers’ degeneracy, the surface spectrum has two dimensional *Dirac points* at  $\Lambda_a$ . The *relative* values of  $\pi_a = \delta_{a1} \delta_{a2}$  determine how these Dirac points are connected to one another, as illustrated in Fig. 1. For any path connecting  $\Lambda_a$  to  $\Lambda_b$ , the surface band structure will resemble Fig. 1a (1b) for  $\pi_a \pi_b = -1 (+1)$ , and the surface bands will intersect the Fermi energy an odd (even) number of times. It follows that the surface Fermi arc divides the surface Brillouin zone into two regions. The Dirac points at the TRIM  $\Lambda_a$  with  $\pi_a = +1$  are on one side, while those with  $\pi_a = -1$  are on the other side.

In Fig. 2 we depict  $\delta_i$  for four different topological classes, along with the predictions for the edge state spectrum for a 001 face. The surface Fermi arc encloses either 0(4), 1(3), or 2 Dirac points. When the number of Dirac points is not 0(4), there *must* be surface states which connect the bulk conduction and valence bands.

There are two classes of phases depending on the parity of  $\nu_0$ . For  $\nu_0 = 0$  each face has either 0(4) or 2 enclosed Dirac points. For a face  $\mathbf{G} = \sum_i m_i \mathbf{b}_i$  there are 0(4) Dirac points for  $m_i = \nu_i \bmod 2$  ( $i = 1, 2, 3$ ) and 2 Dirac points otherwise. These phases can be interpreted as layers of 2D QSH states stacked in the  $\mathbf{G}_\nu$  direction. They resemble three dimensional quantum Hall phases[14], which are indexed by a triad of Chern integers that define a reciprocal lattice vector  $\mathbf{G}$  perpendicular to the layers and give the conductivity  $\sigma_{ij} = (e^2/h) \varepsilon_{ijk} G_k / (2\pi)$ . In the present case,  $\mathbf{G}_\nu$  is defined modulo  $2\mathbf{G}$ , so that layered QSH phases stacked along  $\mathbf{G}_\nu$  and  $\mathbf{G}_\nu + 2\mathbf{G}$  are equivalent.

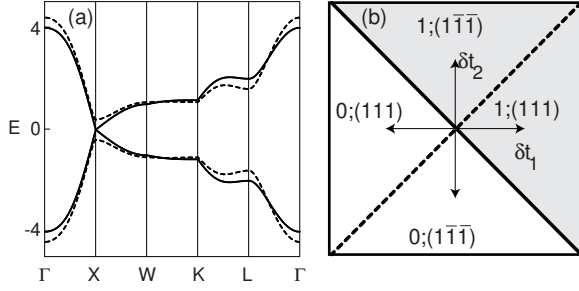


FIG. 3: Energy bands for (a) the model (4) with  $t = 1$ ,  $\lambda_{SO} = .125$ . The symmetry points are  $\Gamma = (0, 0, 0)$ ,  $X = (1, 0, 0)$ ,  $W = (1, 1/2, 0)$ ,  $K = (3/4, 3/4, 0)$  and  $L = (1/2, 1/2, 1/2)$  in units of  $2\pi/a$ . The dashed line shows the energy gap due to  $\delta t_1 = .4$ . (b) shows the phase diagram as a function of  $\delta t_1$  and  $\delta t_2$  (for bonds in the 111 and  $1\bar{1}\bar{1}$  directions) with phases indexed according to cubic Miller indices for  $\mathbf{G}_\nu$ . The shaded region is the STI phase.

The presence or absence of surface states in the  $\nu_0 = 0$  phases is delicate. For the  $0;(001)$  phase in Fig. 2, the 100 face has two Dirac points, while the 801 face has 0(4). This sensitivity is a symptom of the fact that the topological distinction of these phases relies on the translational symmetry of the lattice. Indeed, if the unit cell is doubled, the two Dirac points fold back on one another. A weak periodic potential then opens a gap. It is thus likely that disorder will eliminate the topological distinction between these phases and simple insulators. Surface states will generically be localized. For this reason, we refer to the  $\nu_0 = 0$  phases as “weak” topological insulators. Nonetheless, the weak invariants have important implications for clean surfaces.

The  $\nu_0 = 1$  phases are more robust, and we refer to them as “strong” topological insulators. In this case the surface Fermi arc encloses 1(3) Dirac points on *all* faces. If the Fermi energy is exactly at the Dirac point this provides a time reversal invariant realization of the 2+1 dimensional parity anomaly[15, 16, 17, 18] *without fermion doubling*. This can occur because the Dirac point partners reside on opposite surfaces. For a generic Fermi energy inside the bulk gap the surface Fermi arc will enclose a single Dirac point. This defines a two dimensional “topological metal” that is topologically protected because a quantized Berry’s phase of  $\pi$  is acquired by an electron circling the Fermi arc. This Berry’s phase implies that with disorder the surface is in the symplectic universality class[19, 20], which is not localized by weak disorder.

To develop an explicit model of these phases we consider a 4 band tight binding model of  $s$  states on a diamond lattice with SOI, that generalizes the 2D honeycomb lattice model[5, 16, 18].

$$H = t \sum_{\langle ij \rangle} c_i^\dagger c_j + i(8\lambda_{SO}/a^2) \sum_{\langle\langle ij \rangle\rangle} c_i^\dagger \mathbf{s} \cdot (\mathbf{d}_{ij}^1 \times \mathbf{d}_{ij}^2) c_j. \quad (4)$$

The first term is a nearest neighbor hopping term connecting the two fcc sublattices of the diamond lattice. The second term connects second neighbors with a spin dependent amplitude.  $\mathbf{d}_{ij}^{1,2}$  are the two nearest neighbor bond vectors traversed between sites  $i$  and  $j$ .  $a$  is the cubic cell size. The energy bands are shown in Fig. 3a. Due to inversion symmetry, each band is doubly degenerate. The conduction and valence bands meet at 3D Dirac points at the three inequivalent X points  $X^r = 2\pi\hat{r}/a$ , where  $r = x, y, z$ . This degeneracy is lifted by symmetry lowering modulations of the four nearest neighbor bonds  $t \rightarrow t + \delta t_p$ , with  $p = 1, \dots, 4$ .

Near  $X^z$  the low energy effective mass model has the form of a 3+1 dimensional Dirac equation,

$$\mathcal{H}_{\text{eff}}^z = t a \sigma^y q_z + 4\lambda_{SO} a \sigma^z (s^x q_x - s^y q_y) + m^z \sigma^x. \quad (5)$$

Here  $\mathbf{q} = \mathbf{k} - X^z$  and  $m^z = \sum_p \delta t_p \text{sgn}[\mathbf{d}_p \cdot \hat{z}]$ .  $\mathbf{d}_p$  is the bond vector associated with the  $p$ ’th nearest neighbor bond. The Pauli matrices  $\sigma^i$  are associated with the sublattice degree of freedom, while  $s^i$  describe the spin.  $\mathcal{H}_{\text{eff}}^{x,y}$  are the same with  $x, y$  and  $z$  permuted in  $q_i$  and  $s^i$ , but not  $\sigma^i$ . Transitions between different phases occur when the masses at any of the  $X^r$  vanish.  $\delta t_p = 0$  is thus a multicritical point separating 8 different time reversal invariant phases.

Determining  $\nu_i$  for these phases using (1-3) requires eigenvectors that are defined continuously throughout the Brillouin zone[12]. Since the Chern integers vanish, this is always possible. Determining the appropriate phases numerically, however, is nontrivial. An alternative (though tedious) numerical approach would be to characterize the Pfaffian function introduced in Ref. 6. Generalizing the results of Ref. 12 it can be shown that the product of 4  $\delta_i$  in any plane is related to the zeros of the Pfaffian in that plane, which can be identified without choosing phases. For the present problem, however, we are fortunate because the eigenvectors can be determined analytically, allowing for the continuation of  $w_{ij}(\mathbf{k})$  between the different  $\Gamma_i$ . We find

$$\delta_i = \text{sgn} \left[ \sum_p (t + \delta t_p) \cos \Gamma_i \cdot (\mathbf{d}_p - \mathbf{d}_1) \right]. \quad (6)$$

For small  $\delta t_p$ ,  $\delta = 1$  at  $\mathbf{k} = 0$  and at 3 of the L points.  $\delta = -1$  at the 4th L point. At  $X^r$ ,  $\delta = \text{sgn}[m^r]$ . When one of the four bonds is weaker than the others ( $\delta t_p < 0$ ,  $\delta t_{(p' \neq p)} = 0$  for instance) the system is in a WTI phase, which may be interpreted as a QSH state layered in the  $\mathbf{d}_p$  direction. There are 4 such states, depending on  $p$ , of which two are shown in Fig. 3b. We labeled the phases with the conventional cubic Miller indices for  $\mathbf{G}_\nu$ . 111 and  $1\bar{1}\bar{1}$  are distinct elements of the fcc mod 2 reciprocal lattice. When one of the bonds is stronger than the others the system is in one of four STI phases. The band insulator  $0;(000)$  is not perturbatively accessible from this critical point. However, in the tight binding model

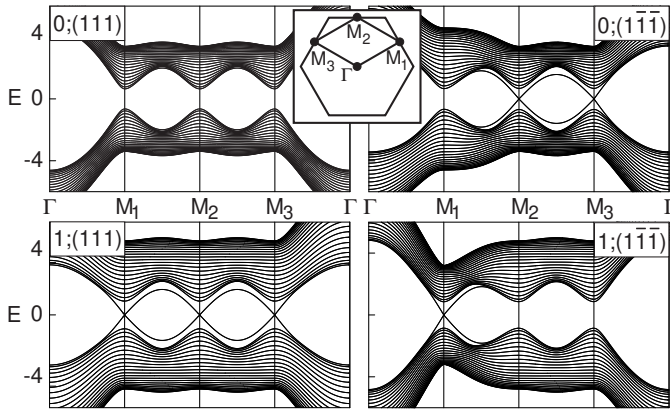


FIG. 4: 2D band structures for a slab with a 111 face for the four phases in Fig. 3. The states crossing the bulk energy gap are localized at the surface. In the WTI (STI) phases there are an even (odd) number of Dirac points in the surface spectrum. The inset shows the surface Brillouin zone.

it occurs when one bond is turned up so that  $\delta t_1 > 2t$ . A staggered sublattice potential also leads to a band insulator, but the strength must exceed a finite value (set by  $\lambda_{SO}$ ) before that transition occurs.

To study the surface states, we solve (4) in a slab geometry. Fig. 4 shows the 2 dimensional band structures of the four phases in Fig. 3 for a slab parallel to the 111 surface along lines that visit each of the four TRIM. The plots with the same  $\nu_0$  can be viewed as different faces of the same state. The bulk states above the bandgap are clearly seen. In addition, there are surface states which traverse the gap. In the WTI phases  $0;(111)$  and  $0;(\bar{1}\bar{1}\bar{1})$  there are 0 and 2 2D Dirac points, on both the top and bottom surfaces, as expected from the general arguments given above. In the STI phases  $1;(111)$  and  $1;(\bar{1}\bar{1}\bar{1})$  there is 1(3) Dirac point on each surface. In each case, the non degenerate surface states near the Dirac points are spin filtered, such that  $\langle \vec{s}(-\mathbf{k}) \rangle = -\langle \vec{s}(\mathbf{k}) \rangle$ . Spin density and charge current are thus coupled.

Though the 4 band diamond lattice model is simple, it is probably not directly relevant to any specific material. However, it may give insight into the behavior of real crystals. Consider a sequence of crystal structures obtained from diamond by continuously displacing the fcc sublattices in the (111) direction:

$$\text{diamond} \rightarrow \text{graphite(ABC)} \rightarrow \text{cubic.}$$

Starting with diamond, the 111 nearest neighbor bond is stretched, leading to the  $0;(111)$  WTI phase. As the sublattice is displaced further both sublattices eventually reside in the same plane with a structure similar to ABC stacked graphite. Displacing further, the lattice eventually becomes cubic. At this point, the gap closes, and the system is metallic. The  $s$  state model remains in the WTI phase up to the cubic point.

Bismuth has the rhombohedral A7 structure, which can be viewed as a cubic lattice distorted “toward diamond”, along with a trigonal distortion of the fcc Bravais lattice. Murakami showed that a bilayer of bismuth, whose structure is similar to a single plane of graphene, is in the QSH phase. This suggests that for weak coupling between bilayers bismuth is in the  $0;(111)$  WTI phase. While this agrees with the simple model presented above, a realistic description of bismuth requires a theory which incorporates bismuth’s five valence bands[21].

It will be interesting to search for materials in the STI phase, which occur on the “other side of diamond” in our sequence. We hope that the exotic surface properties predicted for this phase will stimulate further experimental and theoretical efforts.

It is a pleasure to thank Joel Moore and Leon Balents for helpful discussions. This work was supported by NSF grants DMR-0079909 and DMR-0605066 and DOE grant DE-FG02-ER-0145118.

*Note added:* In subsequent work we have predicted that a number of specific materials are STI’s[22]. These include the semiconducting alloy  $\text{Bi}_{1-x}\text{Sb}_x$  as well as  $\alpha$ -Sn and HgTe under uniaxial strain.

- 
- [1] S. Murakami, N. Nagaosa and S.C. Zhang, Science **301**, 1348 (2003).
  - [2] J. Sinova et al., Phys. Rev. Lett. **92**, 126603 (2004).
  - [3] Y.K. Kato et al., Science **306**, 1910 (2004).
  - [4] J. Wunderlich, B. Kaestner, J. Sinova, T. Jungwirth, Phys. Rev. Lett. **94** 047204 (2005).
  - [5] C.L. Kane and E.J. Mele Phys. Rev. Lett. **95** 226801 (2005).
  - [6] C.L. Kane and E.J. Mele Phys. Rev. Lett. **95** 146802 (2005).
  - [7] D.J. Thouless, M. Kohmoto, M.P. Nightingale and M. den Nijs, Phys. Rev. Lett **49**, 405 (1982).
  - [8] Y. Yao, et al., cond-mat/0606350 (2006); H. Min, et al., cond-mat/0606504 (2006).
  - [9] S. Murakami, cond-mat/0607001 (2006).
  - [10] J.E. Moore and L. Balents, cond-mat/0607314 (2006).
  - [11] R. Roy, cond-mat/0607531 (2006).
  - [12] L. Fu and C.L. Kane, Phys. Rev. B **74**, 195312 (2006).
  - [13] R.B. Laughlin, Phys. Rev. B **23**, R5632 (1981).
  - [14] M. Kohmoto, B.I. Halperin and Y.-S. Wu, Phys. Rev. B **45**, 13488 (1992).
  - [15] R. Jackiw, Phys. Rev. D **29**, 2375 (1984).
  - [16] G.W. Semenoff, Phys. Rev. Lett. **53**, 2449 (1984).
  - [17] E. Fradkin, E. Dagotto, D. Boyanovsky, Phys. Rev. Lett. **57**, 2967 (1986).
  - [18] F.D.M. Haldane, Phys. Rev. Lett. **61**, 2015 (1988).
  - [19] H. Suzuura and T. Ando, Phys. Rev. Lett. **89** 266603 (2002).
  - [20] S. Hikami, A.I. Larkin and Y. Nagaoka, Prog. Theor. Phys. **63**, 707 (1980).
  - [21] Y. Liu and R.E. Allen, Phys. Rev. B **52**, 1566 (1995).
  - [22] L. Fu and C.L. Kane, cond-mat/0611341 (2006).